Journal of Luminescence 258 (2023) 119789

Contents lists available at ScienceDirect

Journal of Luminescence

journal homepage: www.elsevier.com/locate/jlumin

Full Length Article

Two excitation pathways of Pr^{3+} ion emission in HfO_2:Si:Pr films depending on crystalline phase transformations in annealing

M.A. Garcia Andrade [a], T. Torchynska [b,*], J.L. Casas Espinola [b], E. Velázquez Lozada [c], G. Polupan [c], L. Khomenkova [d,e,f], F. Gourbilleau [e]

[a] Instituto Politécnico Nacional – ESIME Cul. México City, 04260, Mexico
[b] Instituto Politécnico Nacional - ESFM, México City, 07738, Mexico
[c] Instituto Politécnico Nacional – ESIME Zac, México City, 07738, Mexico
[d] V. Lashkaryov Institute of Semiconductor Physics at NASU, Kyiv, 03028, Ukraine
[e] CIMAP, UMR CNRS/CEA/ENSICAEN/UNICAEN, 14050, Caen, Cedex 4, France
[f] National University "Kyiv-Mohyla Academy", Kyiv, 04170, Ukraine

A R T I C L E I N F O

Keywords:
Si rich HfO2:Pr films
Rare earth (RE) ion Pr3+
Bright emission
Two excitation pathways

A B S T R A C T

The impact of annealing on the emission and transformation of the crystalline phases in Si rich HfO_2:Pr films was investigated by analyzing the morphology, chemical composition, structure, and photoluminescence (PL) characteristics. Films were prepared by RF magnetron sputtering and monitored as-prepared and after annealing at 1000 °C for 5–60 min. Emission through host HfO_2 defects has only been detected in spectra of as-prepared Si rich HfO_2:Pr films. Heat treatment for 30 min stimulates a phase transformation together with the appearance of a tetragonal HfO_2 phase and Si quantum dot (QDs). This last process is accompanied by appearance of bright emission of rare earth (RE) ions Pr^{3+} related to the transitions in the 4f energy levels. Additional annealing for 60 min stimulates the complete oxidation of the Si QDs with the formation of the SiO_2 phase along with partial destruction of a tetragonal HfO_2 phase. This last process is accompanied by the significant increase of the intensity of Pr^{3+} ion emission. Two forms of luminescence excitation in 4f energy levels of Pr^{3+} ions are discussed, related to energy transfer to Pr^{3+} ions, first from Si QDs and then from host defects in HfO_2. These changes in the excitation pathways of Pr^{3+} ion emissions are stimulated by the transformations of the crystalline phases in the thermal treatment together with the generation of host HfO_2 defects. Hafnia-based materials doped with RE elements are interesting for telecommunication technology and applications in waveguides and optoelectronic devices.

1. Introduction

Hafnia-based materials have aroused great scientific interest, initially due to the high refractive index (about 2.0 at 1.95 eV) that promise their applications as alternative dielectrics to SiO_2 in CMOS technology [1,2] or in silica-hafnia waveguides [3,4]. Other advantages of HfO_2 relate to its large band gap (≈5.8–6.0 eV) and high transparency in the ultraviolet–visible–infrared spectral ranges that allow this material to be used in photonics and optoelectronics [5–7].

Photoluminescence (PL) of undoped HfO_2 films was previously detected in ultraviolet (4.0–4.2 eV) and visible (2.5–3.5 eV) spectral ranges [8,9]. UV luminescence related to exciton emission almost disappeared at 300 K. The visible emission of HfO_2 at 300 K was attributed to recombination through host defects, such as oxygen vacancies with trapped electrons in the HfO_2 matrix [8–10]. Furthermore, the HfO_2 material is attractive for doping with various elements, which produce radiative emission centers in the HfO_2 matrix.

The great demand for optical sources and amplifiers operating in telecommunication wavelengths for fiber optic communication technology stimulated attention towards hafnia-based materials doped with rare earth (RE) elements [7]. Recently, a set of articles related to the emission investigation of HfO_2 films doped with RE elements Nd, Er, Pr … etc was presented [7,11–19]. The emission of trivalent RE ions, such as Er^{3+}, in the green ($4S_{3/2} \rightarrow 4I_{15/2}$) and infrared ($4I_{13/2} \rightarrow 4I_{15/2}$) spectral ranges is important for optic communication technology, as well as an eye-safe source in atmosphere, laser radar, medical and

* Corresponding author.
E-mail address: ttorchynska@ipn.mx (T. Torchynska).

https://doi.org/10.1016/j.jlumin.2023.119789
Received 18 January 2023; Accepted 6 March 2023
Available online 15 March 2023
0022-2313/© 2023 Elsevier B.V. All rights reserved.

surgery applications [20,21]. However, a set of articles related to the investigation of HfO_2 films doped with RE ions is not numerous.

Furthermore, Si-rich-HfO_2 materials, considered for microelectronic applications, have been studied in some papers [11–14,16], but the detailed mechanism of RE ion excitation has not been reported. Moreover, the excitation of RE ion emission, its interaction with host HfO_2 defects and the dependence of RE ion emission on the crystalline phase of HfO_2 matrix are still unclear. This paper is related to the investigation of the crystalline phase variation in the Si-rich hafnia oxide system with annealing at a high temperature and the influence of this process on the emission through the 4f energy levels of Pr^{3+}ions.

2. Experimental details

Pr-doped Si-rich HfO_2 films have been prepared by radio frequency (RF) magnetron sputtering on (100) oriented Si wafers, with 2-in diameter, B-doped with an electrical resistivity of 15 Ω cm. The substrates prior to deposition were subjected to standard RCA clean-up [12]. HfO_2 targets have been used together with the Si and Pr_2O_3 pellets, each covering 2% of the target surface area. Si-HfO_2:Pr films were deposited in Ar plasma at a flux 3 sccm on the Si substrate heated at 400 °C for 150 min. Film deposition was performed with an RF power of 0.74 W/cm^2, a plasma pressure of 0.039 mbar, and a substrate-cathode distance of 57 mm. Then, a substrate with the HfO_2 film was divided into the pieces of 1 × 1 cm^2. The annealing of these pieces was performed in a horizontal furnace at a temperature of 1000 °C for different times of 5, 15, 30 and 60 min under a continuous flow of nitrogen.

Various techniques have been applied to analyse the film characteristics. To control the surface morphology and obtain a micro analysis of the film compositions, a scanning electronic microscope (SEM), model Quanta 3D FEG-FEI, was applied with an Apollo X10 EDAX detector for energy dispersive (EDS) spectroscopy. X-ray diffraction (XRD) measurements was provided on a Model XPERT MRD equipment with an angular resolution of 0.0001° using X-ray (K_{a1} line, λ = 1.5406 Å) obtained from the Cu source.

PL spectra were recorded by a SPEX 500 spectrometer coupled with a photomultiplier Hamamatsu for the visible spectral range or a germanium detector for the IR spectral range. PL was excited by a 325 nm line of a He–Cd laser (model IK3102R-G).

The X-ray photoelectron spectroscopy (XPS) has been applied to monitor the composition of the Si phase in the films using Thermo Scientific™ K-Alpha™ equipment with X-rays of an Al anode (K-alpha line of 1486.7eV), at a voltage of 15 kV (90 W) and a pressure of 1.33 × 10^{-7}Pa. The X-ray beam from a 400 μm spot has been fixed at two energy modes of 40 and 160 eV. XPS spectra were analyzed using Thermo Avantage V5.938 software.

3. Experimental results and discussion

The surface morphology of annealed films is shown in Fig. 1, which depends on the annealing conditions. The film annealed for 5 min shows a surface with mean grain sizes of 28 ±7 nm (Fig. 1a). By increasing the annealing time to 15 min, the mean grain size enlarges to 43.8 + 9.7 nm (Fig. 1b). With increasing the annealing time to 60 min, the mean grain size rises to 56.2 + 15.3 nm (Fig. 1c) and nanocrystals form the clusters separated by valleys (Fig. 1 b, c).

EDS spectroscopy has been used to monitor the chemical compositions of the films. The EDS spectra of the as-deposited and annealed films are presented in Fig. 2. The signals of the Hf, Si, O, Pr, and C elements (Fig. 2) were detected. After heat treatments for 5–30 min, the carbon signal initially disappeared, but after 60 min of annealing, the carbon peak appeared again. The latter may be related to the absorption of carbon from the atmosphere with annealing.

The intensities of the Hf, Si and Pr signals did not change with annealing. Simultaneously, the intensity of the O signal increased significantly (Fig. 2). Therefore, thermal annealing leads to the variation of the chemical composition due to the increase of O content in the films. This latter effect may be related to the fact that it was revealed early in Ref. [22]. It was shown that thermal annealing at 1000 °C in a nitrogen atmosphere of HfSiO thin films caused atomic transport of O and N elements into the films [22].

The XRD patterns recorded for the as-deposited and annealed films are presented in Fig. 3. The films in the as-deposited state show a set of different groups of XRD peaks. The peaks 2Θ = 33.229 (1), 47.675 (2), 56.555 (5) and 77.022 (9) correspond to the diffraction on the crystal planes (200), (220), (311), and (331), respectively, in the cubic PrO_2 lattice (ICDD Ref. Code 00-024-1006). Note that cubic PrO_2 material has been used in magnetron sputtering technology.

Two XRD peaks 2Θ = 50.917 (3) and 62.493 (6) are assigned to diffraction in the (402) and (304) planes, respectively, in the hexagonal

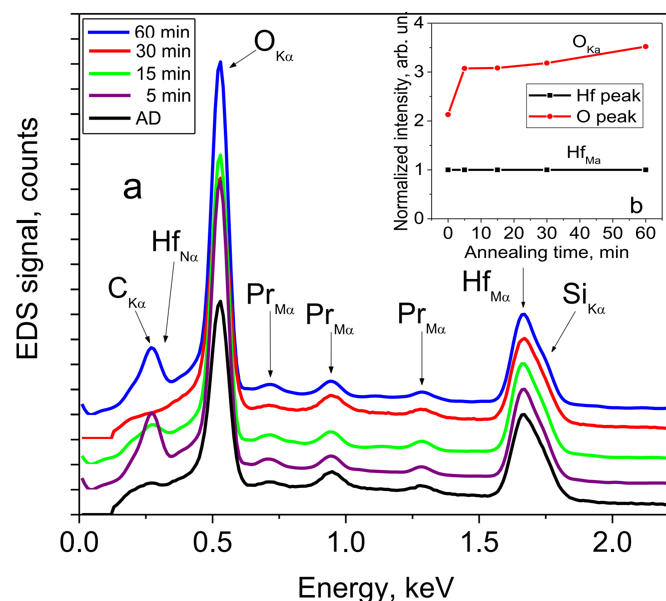

Fig. 2. Normalized EDS results obtained for Si -HfO_2 :P r films: as -deposited and annealed at 1000 °C for 5 –60 min (a). The intensity variation (b) of the O and Hf signals.

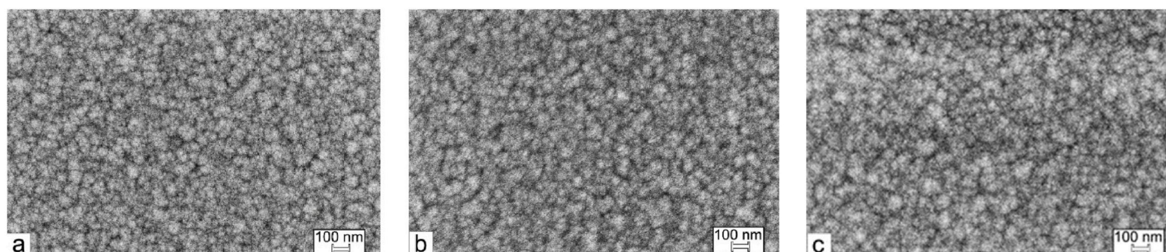

Fig. 1. SEM images of Si-HfO_2:Pr films annealed at 1000 °C for 5 (a), 15 (b), and 60 min (c).

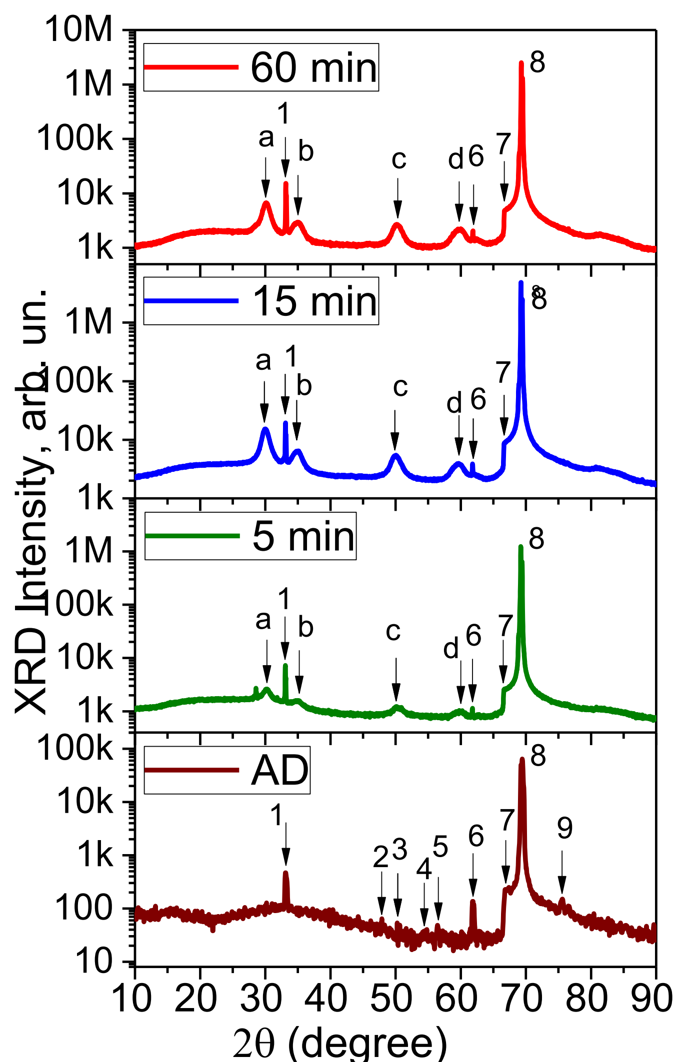

Fig. 3. XRD patterns of the Si-HfO_2:Pr films: as-deposited and annealed at 1000 °C for 5, 15 and 60 min.

lattice of $Pr_2Si_2O_7$ (ICDD Ref. Code 00-023-1389). Two XRD peaks 2ϴ = 53.854 (4) and 68.311 (7) are attributed to diffraction at the (312) and (332) planes, respectively, in the tetragonal lattice of the hafnium silicate $HfSiO_4$ (ICDD Ref. Code 01-075-1628). It means that the crystallization process in the films started while the film was growing on the heated Si substrate (400 °C). The highest XRD peak 2ϴ = 69.440 (8) is related to X-ray diffraction in the Si nanocrystals (Si QDs) and in the Si substrate with the cubic crystal lattice (ICDD Ref. Code 00-005-0565).

Heat treatment stimulates the changes in the XRD pattern (Fig. 3). The peaks 2ϴ = 33.229 (1), 62.493 (6), 68.311(7) and 69.440 (8), connected with diffraction in the praseodymium oxide, praseodymium silicate, hafnium silicate and Si substrate, respectively, have been found as well, but the intensity of peaks related to the Hf and Pr silicates: 2ϴ = 62.493 (6) and 68.311 (7) decreases significantly. The group of new peaks in the XRD patterns was detected at 2ϴ = 30.064° (a), 35.094° (b), 50.345°(c) and 59.684° (d), appearing after 5 min annealing and increasing with rising of the annealing times up to 15–30min. These new peaks are assigned to diffraction in the (101), (200), (220) and (311) planes of the tetragonal HfO_2 crystal structure (ICDD Ref. Code 00-008-0342). NC sizes of HfO_2 in annealed films were estimated using Sharrer's formula [23] in the range of 4.1–4.6 nm. Meanwhile, the XRD intensities of tetragonal HfO_2 related peaks decreased as an annealing time approached 60min (Fig. 3). The latter is related to the initiation of Si QD oxidation with the formation of silicon oxide.

High resolution XPS spectra for the Si2p line in the as deposited and annealed films were investigated to monitor the state of the Si QDs (Fig. 4). The two peaks at 98.5 eV and 101.6 eV are revealed in a HR-XPS spectrum of the as deposited Si-HfO_2:Pr film. These two peaks were assigned to excitation of X-ray photoelectrons of Si atoms located in Si QDs (98.6 eV) and in the chemical composition (101.6 eV) of $HfSiO_x$ [24].

Heat treatment at 1000 °C for 15–30 min stimulated the decrease in the value of the Si2p peak connected with the Si QDs (98.6 eV), together with rising the value of the second peak and its shift to 102.9 eV. These changes testify to oxidation of the Si QDs during annealing at 1000 °C and the beginning of the formation of silicon oxide. Annealing at 1000 °C for 60 min leads to the complete disappearance of the Si2p peak related to Si QDs (98.6eV) and significantly increases the intensity of a Si2p peak belonging to the Si atoms in the SiO_2 lattice together with the peak shift to 103.8 eV [24]. Therefore, the increase of oxygen atoms in the films in thermal annealing at 1000 °C, detected by EDS (Fig. 2b), leads to the oxidation of the Si QDs with the formation of the SiO_2 phase at annealing for 60min (Fig. 4).

The PL spectra measured in the visible and infrared spectral ranges are presented in Figs. 5 and 6 for the Si-HfO_2:Pr films in the as deposited and annealed states.

The as-deposited Si-HfO_2:Pr film shows small intensity visible emission bands with a main peak at 2.78 eV (Fig. 5), but no PL band has been detected in the IR emission spectrum (Fig. 6). Annealing at 1000 °C for 5 min improved the emission intensity in the visible PL range (Fig. 5) but did not change the IR emission spectrum (Fig. 6). The PL spectrum of Si-HfO_2:Pr film annealed for 5 min is very similar to the PL spectrum of the annealed Si-HfO_2 films without the Pr content [8,9]. Therefore, the PL bands related to the emission through the host HfO_2 defects only have been detected in PL spectra of the films after annealing at1000 °C for 5 min.

The deconvolution procedure was applied to the visible spectrum obtained after film annealing for 5min and the five PL bands of the Gaussian shapes related to host HfO_2 defects were revealed with the PL bands peaked at: 1.51, 1.96, 2.27, 2.56 and 2.91eV. Comparison of the PL bands (Fig. 5) with the PL spectra of un-doped HfO_2 films [8,9] allows one to assign these bands to carrier recombination across the different

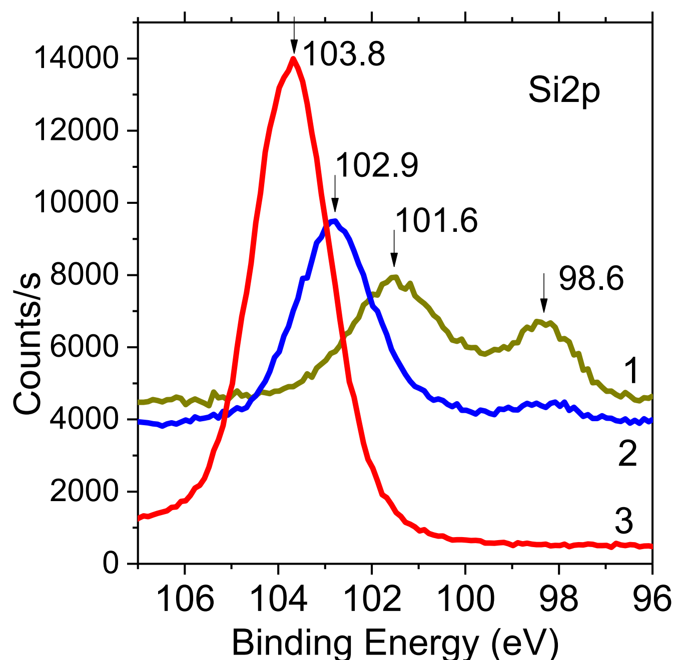

Fig. 4. High resolution XPS spectra obtained for the Si2p lines in the Si-HfO_2:Pr films: as-deposited (1) and annealed at 1000 °C for 30 (2) and 60 (3) min.

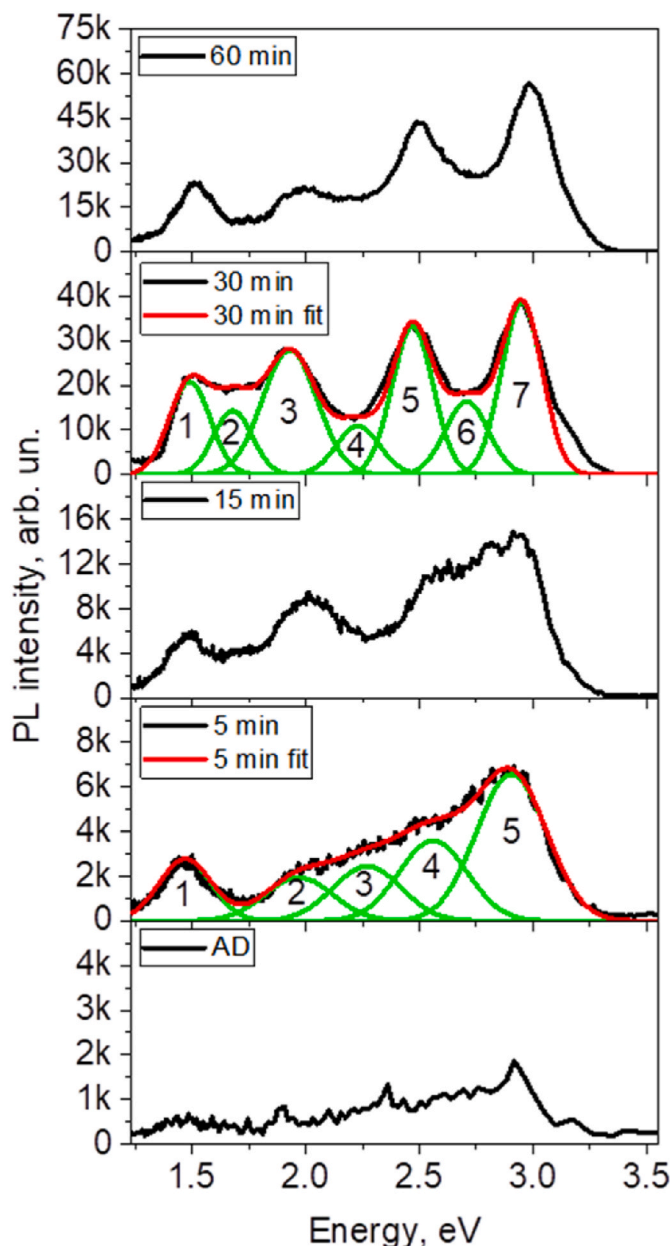

Fig. 5. Visible PL spectra of the Si-HfO_2:Pr films: as-deposited (AD) and annealed at 1000 °C for 5, 15, 30 and 60 min.

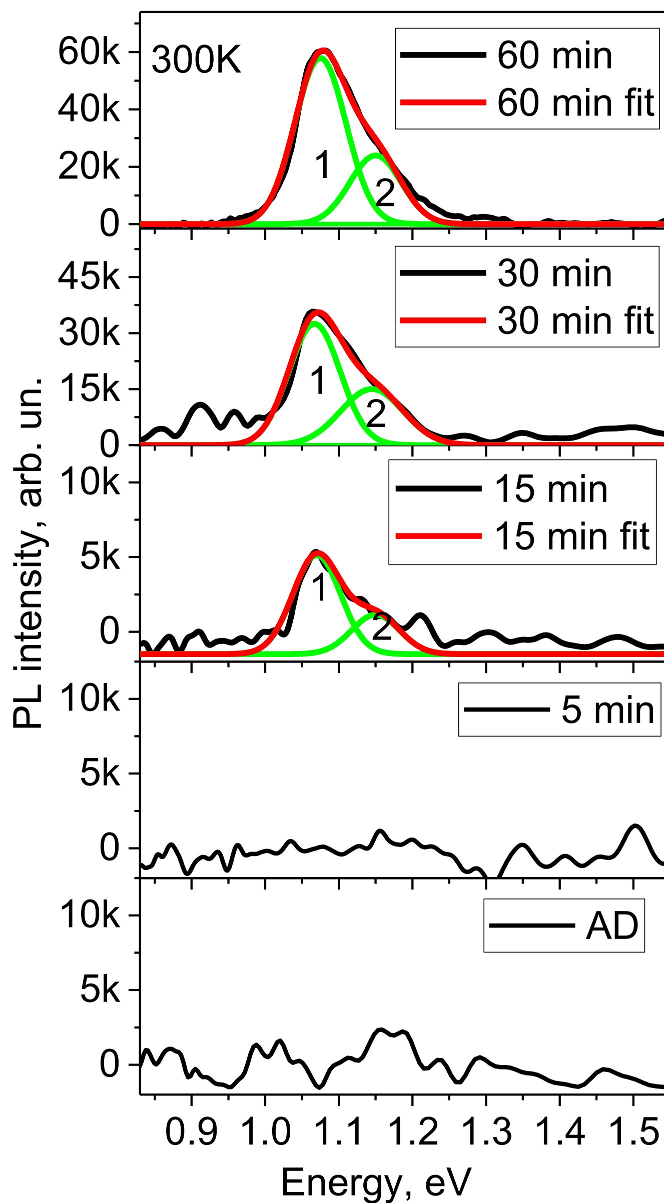

Fig. 6. IR PL spectra of the Si-HfO2:Pr films: as-deposited (AD) and annealed at 1000 °C for 5, 15, 30 and 60 min.

types of electron-trapped oxygen vacancies [8,9].

In XRD patterns of Si-HfO_2:Pr films annealed for 15–60 min, the nanocrystals of the tetragonal HfO_2 structure were detected (Fig. 3). Simultaneously, new PL bands have appeared in the visible and infrared PL spectra (Figs. 5 and 6). Deconvolution was used again at the analysis of the visible and infrared spectra of annealed Si-HfO_2:Pr films (15–60 min) and a series of Gaussian-shaped emission bands related to carrier recombination across internal 4f-4f energy levels of the Pr^{+3} ion, as well as host HfO_2 defects and Si QDs have been revealed (Table 1).

To confirm the nature of the PL bands shown in Table 1, the variation of the integrated intensities of these PL bands with annealing times have been studied (Fig. 7a and b). The appearance of the tetragonal HfO_2 crystalline structure in the films stimulates the increase of the integrated intensities of all PL bands after annealing for 30 min. The latter can be assigned to the improvement of crystallinity and the disappearance of non-radiative recombination centers (NRC) in the films. Simultaneously, the formation of a significant crystalline field stimulates the splitting of the 4f energy levels in Pr^{3+}ions [7]. Furthermore, the correlation exists by varying the PL intensities of the visible peaks P1, P5, P7 (Fig. 7a) and the IR 1 and 2 peaks (Fig. 7b). The latter fact allows us to assign these five bands to the emission transitions within the internal 4f-4f levels in

Table 1
Parameters of VIS and IR PL bands.

The elementary PL bands					
VIS peaks (Fig. 5)	Energy, eV	FWHM, eV	Area	Transition	Reference
1	1.49	0.18	4700	$^1D_2 \rightarrow {}^3F_2$	[25]
2	1.68	0.20	3050	Si QDs	[26]
3	1.93	0.24	8400	Vo	[8,9]
4	2.23	0.19	2600	$^3P_2 \rightarrow {}^3F_2$	[26,27]
5	2.47	0.18	7500	$^3P_0 \rightarrow {}^3H_4$	[26]
6	2.71	0.19	3900	$^3P_2 \rightarrow {}^3H_4$	[27]
7	2.95	0.18	8700	$^1S_0 \rightarrow {}^3P_2$	[26,28]
IR peaks (Fig. 6)					
1	1.08	0.07	5080	$^1D_2 \rightarrow {}^3F_4$	[26,29]
2	1.15	0.07	2100	$^1D_2 \rightarrow {}^3F_3$	[29]

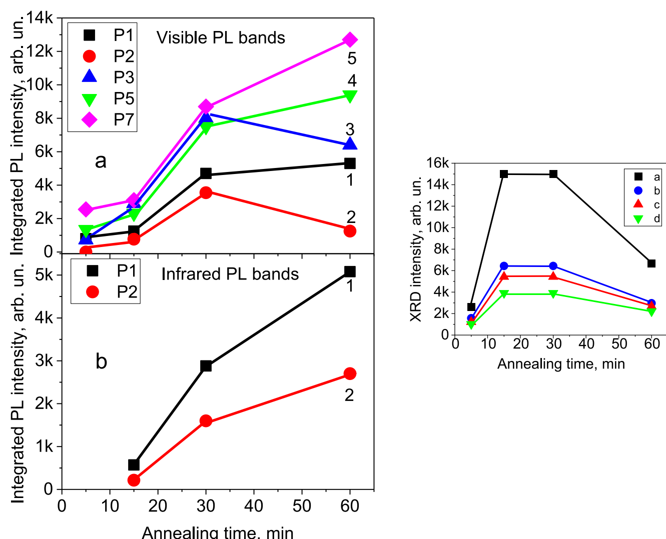

Fig. 7. The variation of integrated PL intensities of the visible (a) and IR (b) PL bands versus annealing time. Fig. 7c. The variation of XRD peak intensities related to diffraction on a-(101), b-(200), c-(220) and d-(311) crystal planes of a tetragonal HfO_2 phase versus annealing times.

the Pr^{+3} ions (Table 1).

Meanwhile, the emission intensity of the P2 peak (Fig. 7a) increases with the annealing time of 30 min owing to the improvement of the crystallinity of the films but decreases significantly with rising the annealing time to 60 min (Figs. 5 and 7a). Simultaneously, as the XPS investigation shows, the intensity of the Si2p line (98.6 eV), related to the Si NCs (Si QDs) decreases (Fig. 4), and completely disappears after annealing for 60 min owing to Si QD oxidation. Analysis of the mentioned data allows us to attribute a PL band 2 to carrier recombination within Si QDs that disappear along with the oxidation of the Si QDs. Therefore, the PL intensity of band 2 increases due to enhancement of film crystallinity and NRC disappearance along with annealing for 30 min, but decreases significantly along with Si QD oxidation with annealing for 60 min.

The cross-section of carrier absorption by RE ions is known to be 10^{-18}-10^{-20} cm^{-2} for 4f-4f levels and the excitation of 4f-4f shell in RE ions requires the excitation energy transition from Si QDs and/or host HfO_2 defects into RE ions. The excitation via Si QDs was widely used for the RE emission stimulation in silica doped with RE ions and with embedded Si QDs [30–34]. The incorporation of Si QDs allows to increase the RE absorption cross-section from 10^{-21} cm^{-2} [35] up to 10^{-16} cm^{-2} [33.34] owing to energy transfer from Si QDs to RE ions (Fig. 8).

Therefore, the inclusion of Si QDs in the HfO_2 film allows, as expected, to obtain an excitation of Pr^{3+} due to the energy transfer from the Si QDs to the RE ions. There is a correlation between the increase in the intensity of the band P2, connected with the Si QDs embedded in the HfO_2 matrix, and the rise of the intensity of PL bands related to the optical transitions within the 4f-4f shell of Pr^{3+}ions: visible P1, P5, P7 and IR 1 and 2 bands in the films annealed for 15–30 min (Fig. 7a and b).

PL peak 3 centered at 1.93 eV in the visible PL spectrum (Fig. 5, Table 1), which increased after annealing at 1000 °C for 15–30 min and decreased after further annealing for 60 min (Fig. 7a) can be assigned to radiative recombination through electron-trapped oxygen vacancies in the HfO_2 films [8,9].

The oxidation of the Si QDs, while annealing the Si-HfO_2:Pr films at 1000 °C for 60 min (Fig. 4), leads to the partial destruction of the tetragonal HfO_2 crystal lattice (Fig. 7c) together with the generation of oxygen vacancies in HfO_2 films. The change in HfO_2 crystallinity is confirmed by the decrease in the intensities of the XRD peaks related to the HfO_2 tetragonal lattice in the films annealed for 60 min (Figs. 3 and

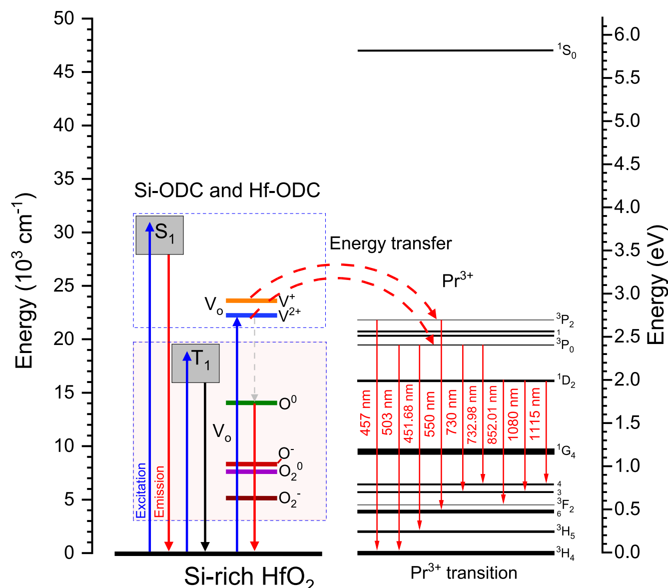

Fig. 8. Energy diagram shows the excitation energy transitions from the Si QDs (Si-ODC) and oxygen vacancies (Hf-ODC) to the 4f energy levels of the Pr^{3+} ions.

7c). Oxygen vacancies, generated in the tetragonal HfO_2 crystal lattice while the Si QD oxidation, then participate in the excitation of Pr^{3+}ion emission through the energy transfer from oxygen vacancies into Pr^{3+}ions (Fig. 8). The last process, as expected, increases the intensity of all emission bands, related to the 4f-4f intra-shell optical transitions in Pr^{3+}ions (Fig. 7a and b), and, simultaneously, decreases the intensity of the emission band P3 connected with oxygen vacancies in the HfO_2 matrix (Fig. 7a). These changes in the intensities of the PL bands related to 4f-4f intra shell emission of Pr $^{3+}$ ions and to emission vis V_O defects we have detected experimentally in the studied films (Fig. 7a and b).

4. Conclusion

The impact of crystalline phase transformation with annealing at a high temperature of 1000 °C on the excitation of emission through the 4f-4f intra-shell optical transitions in the Pr^{3+}ions has been studied in the Si-HfO_2:Pr films. Thermal annealing at 1000 °C for 15–30 min was observed to lead to the formation of the tetragonal HfO_2 crystal lattice together with the Si QD inclusions. Simultaneously, visible and infrared emission has appeared through the 4f-4f shell levels of Pr^{3+}ions. The excitation of this emission is performed due to the energy transfer from the Si QDs to the Pr^{3+} ions.

Annealing at 1000 °C for 60 min is accompanied by the oxidation of Si ODs with the formation of the SiO_2 phase, together with the decrease in the intensity of the PL band P2 of Si QDs (peaked at 1.68 eV). Simultaneously, the partial destruction of an HfO_2 matrix has been performed together with the generation of oxygen vacancies. The last process is characterized by the significant increasing the integrated PL intensities of all PL bands related to emission through 4f-4f intra shell energy levels of Pr^{3+} ions, along with the decrease of the PL intensity of the band P3 related to emission through host defects. In the latter case, the visible-infrared emission of Pr^{3+} ions occur owing to an energy transfer via oxygen vacancies to the Pr^{3+} ions. Our results are interesting for multifunctional applications of Si-HfO_2:Pr films as traditional luminescent phosphors and/or in a telecommunication technology.

Declaration of competing interest

The authors declare that they have no known competing financial interests or personal relationships that could have appeared to influence

the work reported in this paper.

Data availability

Data will be made available on request.

Acknowledgements

This study obtained the financial support of the CONACYT (project 258224) and SIP-IPN (project 20220210) Mexico, as well as the NASU and Ukrainian Ministry of Education and Science, and the French National Agency of Research (ANR).

Supplementary data

The deconvolution of a set of visible and IR spectra was omitted from the main body in the interest of presenting a clearer and more readable manuscript. The mentioned data will be available on request.

References

[1] G. He, L.Q. Zhu, Z.Q. Sun, Q. Wan, L.D. Zhang, Integrations, and challenges of novel high-*k* gate stacks in advanced CMOS technology, Prog. Mater. Sci. 56 (2011) 475–572.
[2] L. Khomenkova, X. Portier, J. Cardin, F. Gourbilleau, Thermal stability of high-k Si-rich HfO2 layers grown by RF magnetron sputtering, Nanotechnology 21 (2010), 285707.
[3] R.R. Gonçalves, G. Carturan, L. Zampedri, M. Ferrari, M. Montagna, A. Chiasera, G. C. Righini, S. Pelli, S.J.L. Ribeiro, Y. Messaddeq, Sol-gel Er-doped SiO2–HfO2 planar waveguides: a viable system for 1.5 μm application, Appl. Phys. Lett. 81 (2002) 28–30.
[4] M. Mattarelli, M. Montagna, F. Rossi, C. Tosello, N.D. Afify, M. Bettinelli, A. Speghini, C. Armellini, Y. Jestin, F. Rocca, S. Gialanella, Raman and Er^{3+} spectroscopy of hafnia single crystals and nanocrystals, Opt. Mater. 31 (2009) 1362–1365.
[5] J.M. Khoshman, A. Khan, M.E. Kordesch, Amorphous hafnium oxide thin films for antireflection optical coatings, Surf. Coat. Technol. 202 (2008) 2500–2502.
[6] O. Stenzel, S. Wilbrandt, S. Yulin, N. Kaiser, M. Held, A. Tünnermann, J. Biskupek, U. Kaiser, Plasma ion assisted deposition of hafnium dioxide using argon and xenon as process gases, Opt. Mater. Express 1 (2011) 278–292.
[7] A.J. Kenyon, Recent developments in rare-earth doped materials for optoelectronics, Prog. Quant. Electron. 26 (2002) 225–284.
[8] L. Khomenkova, Y.-T. An, D. Khomenkov, X. Portier, C. Labbé, F. Gourbilleau, Spectroscopic and structural investigation of undoped and Er3+doped hafnium silicate layers, Phys. B Conds. Matter 453 (2014) 100–106.
[9] R. Demoulin, G. Beainy, C. Castro, P. Pareige, L. Khomenkova, C. Labbé, F. Gourbilleau, E. Talbot, Origin of Pr^{3+} luminescence in hafnium silicate films: combined atom probe tomography and TEM investigations, Nano Futures 2 (2018), 035005.
[10] A.S. Foster, F. Lopez Gejo, A.L. Shluger, R.M. Nieminen, Vacancy and interstitial defects in hafnia, Phys. Rev. B 65 (2002) 1741171–17411713.
[11] V. Kiisk, I. Sildos, S. Lange, V. Reedo, T. Tatte, M. Kirm, J. Aarik, Photoluminescence characterization of pure and Sm^{3+}-doped thin metaloxide films, Appl. Surf. Sci. 247 (2005) 412–417.
[12] T. Torchynska, B. El Filali, L. Khomenkova, X. Portier, F. Gourbilleau, Phase transformation and light emission in Er-doped Si-rich HfO_2 films prepared by magnetron sputtering, JVST A 37 (2019), 031503.
[13] L.X. Liu, Z.W. Ma, Y.Z. Xie, Y.R. Su, H.T. Zhao, M. Zhou, J.Y. Zhou, J. Li, E.Q. Xie, Photoluminescence of rare doped uniaxially aligned nanotubes prepared by sputtering with electrospun polyvinylpyrolidone nanofibers as templates, J. Appl. Phys. 107 (2010), 024309.
[14] T. Torchynska, L.G. Vega Macotela, L. Khomenkova, F. Gourbilleau, Light emission in Nd doped Si-rich HfO_2 films prepared by magnetron sputtering, J. Electron. Mater. 49 (2020) 3441–3449.
[15] G.C. Righini, S. Berneschi, G. Nunzi Conti, S. Pelli, E. Moser, R. Retoux, P. Féron, R. R. Gonçalves, G. Speranza, Y. Jestin, M. Ferrari, A. Chiasera, A. Chiappini, C. Armellini, Er3+-doped silica–hafnia films for optical waveguides and spherical resonators, J. Non-Cryst. Sol. 355 (2009) 1853–1860.
[16] T. Torchynska, L.G. Vega Macotela, L. Khomenkova, F. Gourbilleau, L. Lartundo Rojas, Annealing impact on emission and phase varying of Nd-doped Si-rich-HfO2 films prepared by RF magnetron sputtering, J. Mater. Sci. Mater. Electron. 31 (2020) 4587–4594.
[17] T. Torchynska, L.G. Vega Macotela, G. Polupan, O. Melnichuk, L. Khomenkova, F. Gourbilleau, Raman scattering, emission and crystalline phase evolutions in Nd-doped Si-rich HfO2: N films, J. Mater. Sci. Mater. Electron. 32 (2021) 17473–17481.
[18] L.G. Vega Macotela, T. Torchynska, L. Khomenkova, F. Gourbilleau, Light emission and structure of Nd-doped Si-rich-HfO2 films prepared by magnetron sputtering in different atmospheres, Mater. Chem. Phys. 229 (2019) 263–268.
[19] V. Monteseguro, M. Rathaiah, K. Linganna, A.D. Lozano-Gorrín, M.A. Hernández-Rodríguez, I.R. Martín, P. Babu, U.R. Rodríguez-Mendoza, F.J. Manjón, A. Muñoz, C.K. Jayasankar, V. Venkatramu, V. Lavín, Chemical pressure effects on the spectroscopic properties of Nd^{3+}-doped gallium nano-garnets, Opt. Mater. Express 5 (2015) 1661–1668.
[20] C. Stoneman, L. Esterowitz, Efficient, broadly tunable, laser-pumped Tm:YAG and Tm:YSGG cw lasers, Opt. Lett. 15 (1990) 486–488.
[21] L. Feng, J. Wang, Q. Tang, L.F. Liang, H.B. Liang, Q. Su, Optical properties of Ho^{3+}-doped novel oxyfluoride glasses, J. Lumin. 124 (2007) 187–194.
[22] L. Miotti, K.P. Bastos, G.V. Soares, C. Driemeier, R.P. Pezzi, J. Morais, I.J. R. Baumvol, A.L.P. Rotondaro, M.R. Visokay, J.J. Chambers, M. Quevedo-Lopez, L. Colombo, Exchange-diffusion reactions in HfSiON during annealing studied by Rutherford backscattering spectrometry, nuclear reaction analysis and narrow resonant nuclear reaction profiling, Appl. Phys. Lett. 85 (2004) 4460.
[23] B.D. Cullity, Elements of X-Ray Diffractions, Addison-Wesley, Reading, MA, 1972, p. 102.
[24] NIST X-ray Photoelectron Spectroscopy Database 20, DOI: https://doi.org/10.18434/T4T88K: https://srdata.nist.gov/xps/selEnergyType.aspx.
[25] F. Chun, W. Li, B. Zhang, W. Deng, X. Chu, H. Su, H. Osman, H. Zhang, X. Zhao, W. Yang, Visible and near-infrared luminescent properties of Pr^{3+} doped strontium molybdate thin films by a facile polymer-assisted deposition process, J. Colloid Interface Sci. 531 (2018) 181–188.
[26] Y. An, C. Labbé, L. Khomenkova, M. Morales, X. Portier, F. Gourbilleau, Microstructure and optical properties of Pr3+-doped hafnium silicate films, Nanoscale Res. Lett. 8 (2013) 43.
[27] M. Runowski, P. Woźny, I.R. Martín, V. Lavín, S. Lis, Praseodymium doped YF3: Pr3+ nanoparticles as optical thermometer based on luminescence intensity ratio (LIR)–Studies in visible and NIR range, J. Lumin. 214 (2019), 116571.
[28] A.M. Srivastava, Aspects of Pr3+ luminescence in solids, J. Lumin. 169 (2016) 445–449.
[29] H.P. Labaki, F.H. Borges, F.J. Caixeta, R.R. Gonçalves, Widely dual tunable visible and near infrared emission in Pr3+-doped yttrium tantalate: Pr3+ concentration dependence on radiative transitions from 3P0 to the 1D2, J. Lumin. 236 (2021), 118073.
[30] O. Jambois, F. Gourbilleau, A.J. Kenyon, J. Montserrat, R. Rizk, B. Garrido, Towards population inversion of electrically pumped Er ions sensitized by Si nanoclusters, Opt Express 18 (2010) 2230–2235.
[31] B. Garrido, C. García, S.-Y. Seo, P. Pellegrino, D. Navarro-Urrios, N. Daldosso, L. Pavesi, F. Gourbilleau, R. Rizk, Excitable Er fraction and quenching phenomena in Er-doped SiO_2 layers containing Si nanoclusters, Phys. Rev. B 76 (2007), 245308.
[32] M. Wojdak, M. Klik, M. Forcales, O.B. Gusev, T. Gregorkiewicz, D. Pacifici, G. Franzò, F. Priolo, F. Iacona, Sensitization of Er luminescence by Si nanoclusters, Phys. Rev. B 69 (2004), 233315.
[33] S. Cueff, C. Labbé, J. Cardin, J.-L. Doualan, L. Khomenkova, K. Hijazi, O. Jambois, B. Garrido, R. Rizk, Efficient energy transfer from Si-nanoclusters to Er ions in silica induced by substrate heating during deposition, J. Appl. Phys. 108 (2010), 064302.
[34] A. Podhorodecki, J. Misiewicz, F. Gourbilleau, J. Cardin, C. Dufour, High energy excitation transfer from silicon nanocrystals to neodymium ions in silicon-rich oxide film. Electrochem, Solid-State Lett 13 (3) (2010) K26.
[35] J. Miniscalco, Erbium-doped glasses for fiber amplifiers at 1500 nm, J. Lightwave Technol. 9 (1991) 234–250.